ILKOM Jurnal Ilmiah Vol. 15, No. 3, December 2023, pp. 488-497
Accredited 2nd by RISTEKBRIN No. 200/M/KPT/2020; E-ISSN 2548-7779 | P-ISSN 2087-1716

MobileNet Classifier for Detecting Chest X-Ray Images of COVID-19 based on Convolutional Neural Network

ST Aminah Dinayati Ghani [a,1]; Indo Intan [a,2,*]; Muhammad Rizal [a,3]
[a] *Universitas Dipa Makassar, Jl. P. Kemerdekaan Km. 09, Makassar and 90245, Indonesia*
[1]*dinayati.amy@undipa.ac.id;* [2] *indo.intan@undipa.ac.id;* [3] *muhammad.rizal@undipa.ac.id*
** Corresponding author*

Article history: Received July 04, 2023; Revised August 19, 2023; Accepted December 11, 2023; Available online December 20, 2023

Abstract

Since the COVID-19 pandemic occurred all over the world, numerous studies were carried out to overcome this problem, including COVID-19 image analysis. An expert analysis based on the Chest X-ray images of COVID-19 determines the progression of the lung condition. Eye visualization and expertise of a radiologist have limitations in handling big cases. This study aims to implement the Convolutional Neural Network (CNN) and MobileNet models as deep learning models to classify chest X-ray images into multiclassification, three categories: COVID-19, normal, and virus. The processes were pre-processing and processing. The pre-processing stage was preparing data, and the processing stage was the implementation model and investigating the best model performance in both convolution and classification in depth-wise convolution and batch normalization. The metrics were accuracy, precision, f1-score, and recall. The CNN results of accuracy, precision, recall, and f1-score respectively were 0.94; 0.99; 0.95; and 0.96. The MobileNet results of the metrics were 0.97; 0.98; 0.99, and 0.99. The MobileNet outperforms the CNN results due to depth-wise convolution and batch normalization. Both models contribute to the faster epoch of the best hyperparameter to achieve loss and accuracy convergence. The models are worth recommending to deployment front-end.

Keywords: Chest X-Ray; CNN; COVID-19; Image Analysis; MobileNet.

Introduction

The Coronavirus-19 (COVID-19) is an infectious disease caused by the severe acute Respiratory Syndrome Coronavirus [1]. This virus can attract people who are very easily infected with viruses, COVID-19 is a virus that was first identified in Wuhan, China in December 2019 [2], which then spread throughout China [3], then to other countries around the world which are designated as a pandemic by the World Health Organization (WHO). The term COVID-19 was inaugurated by the WHO on 11 February 2020. In Indonesia, the first case of COVID-19 was identified on 2 March 2020. The symptoms of this virus are coughing, fatigue, fever, headache; body aches and pains, and shortness of breath [4]. Many contactless imaging techniques [5] have been developed during the COVID-19 virus outbreak [6], [7] including one of them is radiological examination or imaging [8].

The protocol for testing whether a subject is infected with COVID-19 must be based on clinical, and epidemiological factors and an assessment of the possibility of infection. One of the tests carried out in the laboratory as a clinical factor is a radiological or imaging examination. Examination efforts have also become the concern of the Ministry of Health and related agencies. One of the examinations that play an important role is chest x-ray radiological examination carried out before the PCR examination. The two results of this examination are carried out sequentially because they mutually reinforce one another [9]. Imaging examination results have an accuracy of more than 90% [8], [10], [11] as good as PCR [12].

The COVID-19 diagnosis method using PCR has high specificity but is also slow, of course, the demand for this examination technique is very high or booming during the pandemic. This examination is the first imaging examination [13] related to symptoms of pneumonia and a Chest X-ray (CXR) test [14]. Radiological examination plays an important role for several reasons, including [15]: a) Time and cost efficiency [11], easy to implement because the results are released quickly and can overcome equipment limitations. In contrast to the results of the RT-PCR examination, it takes quite a long time in the series of examinations [16]; b) An alternative to examinations with negative virological test results, radiological examinations can detect viral infection at an early stage [17].

Radiological examinations carried out so far in several hospitals still use eye visualization and the expertise of a radiologist, therefore, it is common for radiologists to have different analyses. The limited number of health workers, especially radiologists, staff, and expertise is a limiting factor when the number of patients increases. Of course, it results in fatigue, anxiety, boredom, and stress [18]. The effect is that the results of analysis are sometimes inaccurate,

requiring re-examination. This course raises problems such as the accuracy of the examination results is not trusted, protests from the family, and a number of other problems related to the trust and legitimacy of a diagnostic result released by the hospital. The main reason for radiological examination is because it is easy to release and cheap compared to PCR using.

Chest imaging needs to be carried out continuously during the observation or treatment period [19]. The advantage of the CXR examination is that it is available in various hospitals/clinics, and the process is fast, cheap, and affordable for all groups, but the accuracy is less sensitive [10],[20]. Therefore, automated image recognition techniques can be used to assist radiologists in carrying out examinations so that the results are more accurate compared to just using eye visualization.

The approaches used in image recognition are divided into Machine Learning (ML) and Deep Learning (DL) approaches. Both of these approaches have their respective advantages based on their time.

Several ML approaches have been used previously in the digital automatic classification of CXR images [21],[22]. In [23], three statistical features are calculated from lung texture to differentiate between benign and malignant tumors in lung lumps using SVM Classifier. Grey level-co-occurrence matrix combines with back propagation [24] to classify normal cancer images.

The approach using DL has shown its superiority far exceeds the performance of ML [13],[25],[26]. The CNN architecture is the most popular DL approach in the medical imaging domain [27]. The main success of CNNs is due to the ability to automatically recognize features from specific image domains. Unlike ML classification, in CNN architecture training, the strategy is to transfer the trained knowledge from a pre-trained network that is satisfied from one task to the next [13]. Therefore, researchers tend to apply this strategy, especially to medical imaging examinations [13].

The DL method is a representation learning method with multi-level presentation, obtained through the arrangement of simple non-linear modules where each transformation is representative at a low level to a high-representation or very simple abstract level that imitates the human brain [28],[29]. Because the existence of DL models as a breakthrough in artificial intelligence is increasingly being accepted by society for various applications in the field of image recognition [27]. The utility of DL as an ML and pattern recognition tool is also a very important aspect in the field of medical image analysis [30], where its significant impact in the medical imaging domain needs to be investigated [20].

COVID-19 research using CNN includes [31] designing the model using two convolution layers, two polling layers, and a full-connected layer. The fully connected layers use a Multi-Layer Perceptron (MLP) structure and the activation function uses a Rectifier Linear Unit (ReLU). Adam technique as weight update optimization is utilized resulting the accuracy of 89.58%. Research using the same model was carried out by [32] by investing the effect of epoch on finding the best hyperparameters for several epoch experiments to obtain an accuracy of 95% on train data and 78% on test data. The accuracy value obtained by [33] averaged 96% on test data using other research.

The use of the MobileNet model also in the field of CT COVID-19 chest images includes [34] taking CT COVID-19 chest image objects using the MobileNet model to obtain an accuracy of 98.4%. This figure outperforms previous studies which had lower accuracy.

One of the advantages of MobileNet is its simplified lightweight network [35], which uses CNN to separate networks in depth and reduce parameters and computation. The main advantage of MobileNet is that it has fewer parameters and high classification accuracy compared to CNN [36].

The contribution to the research is the success of investigating the MobileNet model which has better performance than CNN even though MobileNet is based on CNN. The input image object is a feature of the COVID-19 CXR image which has many challenges, including the CXR, it is also better to achieve the best results.

This research is described in the following chapters: The introduction discusses the advantages of radiological examination to develop in MobileNet Model based CNN. The Method explains the datasets and model used including pre-processing, processing, and evaluation. The Results and Discussion describe the results of the model simulation and the evaluation as comparation of both models. The Conclusion provides the achievement of the final research objective of successfully obtaining better performance of both models.

Method

This study uses datasets from https://www.kaggle.com/datasets URL. The total dataset used are 1823 images, consisted of 1,276 train data (375 COVID-19; 468 normal; and 433 virus), 547 validation data (161 COVID-19; 200 normal; and 186 virus). The dataset has varying images sizes such as size of images are 776×1168, 1945×2214, and

the size other in JPEG format. The models resize images into 224×224 pixel as input images which are loaded into the model.

The model design has a structure shown by **Figure 1**. The design consists of two models, CNN and MobileNet. CNN is the basis for MobileNet, while the difference lies in the number and dimensions of the layers.

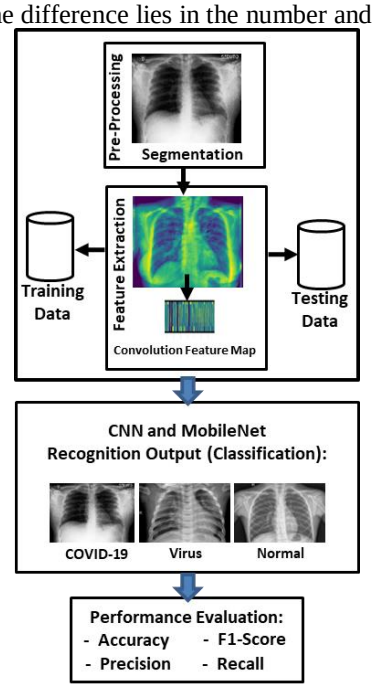

Figure 1. Proposed Stages

The CNN stages as a basis for MobileNet are as **Figure 1**.

The First, **Preprocessing**, performs data acquisition based on multiple classifications, namely COVID-19, normal, and virus, and stores them in the image gallery. There are three folder galleries based on the three classifications. The composition of the prepared image refers to the previous dataset explanation.

The Second, **Processing:**

a. Data acquisition, loading images into the model for reading based on size, image format, and folder access into three folder classes. In this section the medical image is resized referring to an input size of 224×224 pixels. This stage is a segmentation stage by resizing the original image to an image size according to scanning in the input layer of the CNN.

b. Convolution layer, a layer to perform convolution functions as a feature extraction layer. Convolution, $s(t)$ is a vector multiplication between the input image value, $s(t)$ and the kernel, $w(t)$ which experiences horizontal and vertical shifts based on the number of strides (S) and padding (P) as in Equation 1.

$$s(t) = (x \times w)(t) = \sum_{a=\infty}^{\infty} x(a)w(t-a) \quad (1)$$

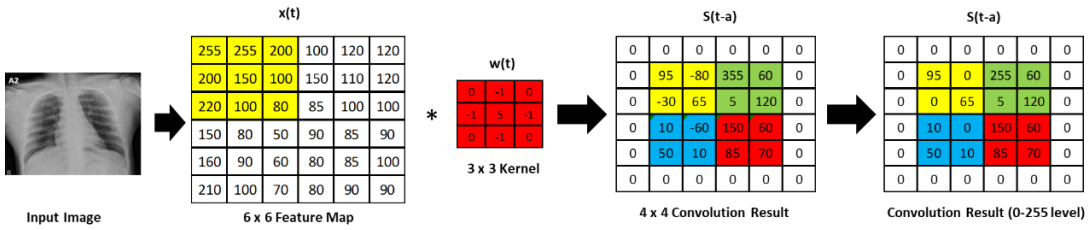

Figure 2. Convolution Layer

The input volume V_i (Equation 2) is the product of width (W_i), height (H_i), and number of channels (C_i) or depth. Output volume (Equation 3) is the result of multiplying width (W_o), height (H_o), and number of channels (C_o) or depth. The (C_i) value refers to the number of basic colors (Red, Green, Blue), and (C_o) refers to the number of K kernels. To determine the convolution layer parameters, refer to (Equation 2 to 6). **Figure 3** shows the convolutional feature output.

$$V(i) = (W_i \times H_i \times C_i) \quad (2)$$

$$V(o) = (W_o \times H_o \times C_o) \quad (3)$$

$$W(o) = \frac{W_i - F + 2P}{S} + 1 \quad (4)$$

$$H(o) = \frac{H_i - F + 2P}{S} + 1 \quad (5)$$

$$C(o) = K \quad (6)$$

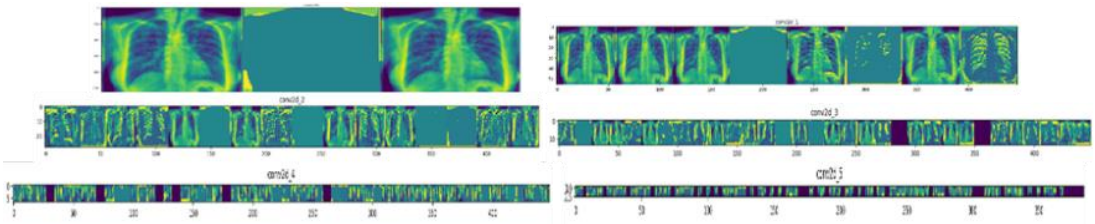

Figure 3. Convolution Feature Extraction

c. Pooling layer, functions to reduce the size of the spatial representation so as to reduce the number of parameters and calculations called sub sampling which is still feature extraction, and also controls overfitting [32].The pooling layer used is Max Pooling by taking the highest convolution value from all vector values calculated as input to the kernel.

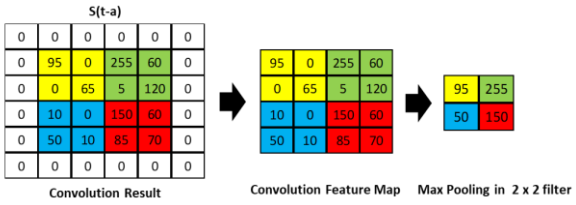

Figure 4. Max Pooling Layer

The feature extractor results appear in the Feature Maps visualization results. The input image is processed in the first convolution layer with a size of 224 × 224 pixels and uses 3 filters. The formula used simulates model equation in Equation 2 to 6. The process of the first convolution can be seen in **Figure 4**. In the initial conditions, image two from the left uses a feature map using NOT logic to mark the boundaries of the CXR with the background image.

The convolution-1 layer takes 224×224 image input-output and then proceeds to max pooling which has input-output 224×224 → 112×112 and has 3 filters. The second convolution takes input-output 112×112 → 112×112, 3 input filters, and 8 output filters, max pooling input-output 112×112 → 56×56, and so on until convolution layer 6 with input-output 7×7 pixels and max pooling input-output 7×7 → 3×3 pixels which have 128 filters, so that 1152 features are formed.

The next stage is flattening to unify all the features in a row vector or column vector for dense and dropout still using all the features in the input-output of 1152 features. After passing through the dropout, it is passed to the activation function to produce 3 output features as the initial classification of the CNN model for COVID-19 in as many as three classes (**Figure 4**).

d. Fully connected layer, as an output layer whose function is to convert a multidimensional array into a vector. Each neuron in the convolution layer needs to be transformed into one-dimensional data. It is the first stage before it can be included in a fully connected layer. Because this causes the data to lose its spatial information and is not reversible, the fully-connected layer can only be implemented at the end of the network [32]. In this section, the classification process is carried out into three classes: COVID-19, normal, and virus.

The next stage is the feature extraction process which is carried out by the model automatically integrated with CNN. In this case CNN is the feature extractor as well as the classifier. The used formula is shown in Equation 2 to 9. Meanwhile, the feature extraction process from the beginning to the end [37] Output a_{ij} on the layer located (i, j), where convolution, and σ is a non-linear function in the network (Equation 1).

$$a_{ij} = \sigma(WX_{ij} + b) \tag{7}$$

After the convolution operation, pooling is introduced to introduce shifts using Equation 8.

$$S_q^l(i,j) = \frac{1}{4}\sum_{u=0}^{z}\sum_{v=0}^{z} C_q^l(2i-u, 2j-v) \tag{8}$$

The results obtained from the final layer of pooling through fully connected for classification and calculating the output produce (Equation 9).

$$Output = \sigma(W \times f + b) \tag{9}$$

Classification, to label each category class using a neural network as a further process of feature extraction for the CNN model.

$$\hat{y}(i) = \frac{e^{\widehat{output}}}{\sum_1^{labels} e^{\widehat{output}}} \tag{10}$$

Introduction, making a comparison between training data and testing data based on the error threshold value or accuracy threshold value (Equation 10).

$$L = \frac{1}{2}\sum_{i=1}^{\substack{Jumlah\\pola\\trainning}} \left(\hat{y}(i) - y(i)\right)^2 \tag{11}$$

$\hat{y}(i)$ as the target output and $y(i)$ is the output obtained so that the first derivative uses Equations 12 to 15:

$$\Delta W(i,j) = \frac{\partial\left(\frac{1}{2}\sum_{i=1}^{p*}\left(\hat{y}(i) - y(i)\right)^2\right)}{\partial\hat{y}} \cdot \frac{\partial\hat{y}}{\partial W(i,j)} \tag{12}$$

$$p* = \hat{y}(i) - y(i) \times \frac{\partial}{\partial W(i,j)}\left(\sigma\left(\sum_{j=1}^{number\ node} W(i,j) \times f(j) + b(i)\right)\right) \tag{13}$$

$$\Delta W(i,j) = \Delta\hat{y}(i) \times f(j) \tag{14}$$

$$\Delta b = \frac{\partial L}{\partial b(i)} \tag{15}$$

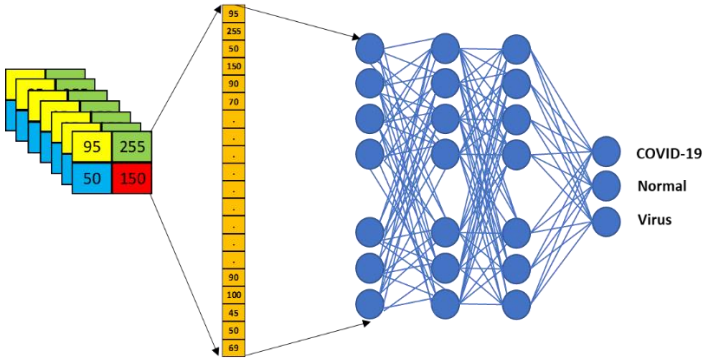

Figure 5. Fully Connected Layer

The Third, **Training process** to obtain the best hyperparameters from the process of obtaining important features in the form of extracts from each data class until a weight value is obtained that corresponds to the data extraction value for each class. Hyperparameters are obtained based on learning rate, epoch, weight of each input based on color image conversion to greyscale (Equation 14) accompanied by data normalization. The goal is to obtain values that require a small memory capacity.

The Fourth, **Testing process** to test the model ability to differentiate between the three classes. The ability of the model to generalize the extraction values for comparison with already stored hyperparameters.

The Fifth, **Evaluation** to compare prediction results and training results, how much image data can be recognized as valid and which is still not valid based on metric measurements based on classification reports (accuracy, precision, F1-score, and recall). This stage also displays the amount of data based on True Positive (TP), False Positive (FP), True Negative (TN), and False Negative (FN).

Confusion matrix is a measure to evaluate the performance of machine learning models and visualize model characteristics in the context of supervised learning [39]. The parameters taken are related to accuracy. Accuracy is the proportion of true predictions which measures how well a classification can predict a condition [38] using Equation 10.

$$Accuracy = \frac{TP + TN}{TP + TN + FP + FN} \quad (16)$$

$$Precision = \frac{TP + TN}{TP + FP} \quad (17)$$

$$F1\ Score = 2 \times \frac{Recall \times Precision}{Recall + Precision} \quad (18)$$

$$Recall = \frac{TP}{TP + FN} \quad (19)$$

Stages 1 to 5 will be carried out by the CNN model and the MobileNet model.

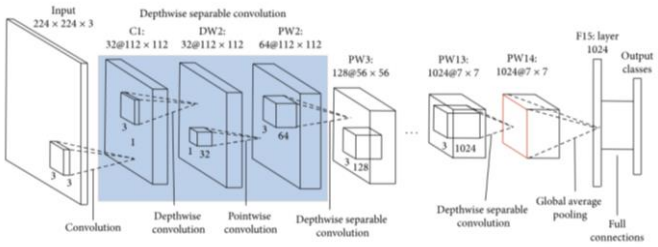

Figure 6. MobileNet Architecture

MobileNet has depth wise separable convolution filters are composed of depth wise convolution filters and point convolution filters. The depth wise convolution filter performs a single convolution on each input channel, and the point convolution filter combines the output of depth wise convolution linearly with 1 × 1 convolution. The process is almost like CNN, but the MobileNet layer requires more layers and other parameters.

The Sixth, **voting** to determine the best performance of both models based on the performance obtained from the evaluation results.

Results and Discussion

Based on the simulated model as described in the Method Section, the author presents the results as follows:

Training Process

The training process uses train data as much as 70% of the dataset based on the composition of the previous data. The CNN model uses the RELU kernel in the input and hidden layer, while the output layer uses SoftMax in Adam optimization. The results obtained show the values in **Table 1**.

In the early epoch, the accuracy value was still low, while the loss value was still high. The simulation uses 15 epochs to train the data to obtain the best accuracy and loss values for both models (**Table 1**). MobileNet as an improvement of CNN layers shows quite significant differentiation values. MobileNet performance outperforms CNN in terms of epoch, step speed, loss, val loss, and val loss as shown in **Table 2**. Even the epoch, step speed, and loss values show very significant numbers because their values are smaller than half of the CNN model values.

Table1. Model Train Results

Epoch	Train Value of CNN Model					Train Value of MobileNet Model				
	Step Speed	*Loss*	*Acc**	*Val loss*	*Val acc**	*Step Speed*	*Loss*	*Acc**	*Val loss*	*Val acc**
1	258	1.0496	0.5765	0.8730	0.6735	134	7.6532	0.7892	1.9684	0.9132
2	133	0.4098	0.8569	0.3688	0.8767	69	0.5471	0.9608	0.7566	0.9384
3	128	0.2427	0.9186	0.3278	0.8813	65	0.0744	0.9863	0.9504	0.9064
4	133	0.1694	0.9422	0.3966	0.8904	69	0.2273	0.9784	0.7548	0.9566
5	136	0.1333	0.9529	0.3061	0.9087	67	0.0163	0.9971	0.6208	0.9612
6	134	0.0698	0.9775	0.3003	0.9132	65	3.0818e-04	1.0	0.6370	0.9566
7	135	0.0852	0.9676	**0.2490**	0.9064	67	4.0846e-05	1.0	**0.6174**	0.9612
8	129	0.0709	0.9765	0.2656	0.9087	65	8.4775e-06	1.0	0.6182	0.9612

Epoch	Train Value of CNN Model					Train Value of MobileNet Model				
	Step Speed	*Loss*	*Acc**	*Val loss*	*Val acc**	*Step Speed*	*Loss*	*Acc**	*Val loss*	*Val acc**
9	130	0.0701	0.9755	0.3432	0.8927	68	5.3142e-06	1.0	0.6184	0.9589
10	135	0.0642	0.9784	0.4829	0.8881	68	4.2823e-06	1.0	0.6184	0.9612
11	136	0.0603	0.9735	0.4274	0.9018	66	3.6169e-06	1.0	0.6175	0.9612
12	136	0.0427	0.9882	0.3498	0.9064	69	1.1773e-05	1.0	0.6183	0.9612
13	132	0.0160	0.9922	0.3445	**0.9315**	**65**	3.5722e-06	1.0	0.6186	0.9612
14	**131**	**0.0152**	**0.9951**	0.5171	0.9247	68	3.2675e-06	1.0	0.6188	**0.9612**
15	137	0.0363	0.9873	0.4183	0.9041	68	**2.8701e-06**	**1.0**	0.6188	0.9589

*Accuracy

Table 2. Comparison of Model Performance

Model	Epoch	Step Speed	Loss	Accuracy	Val loss	Val acc
CNN	14	131	0.0152	0.9951	0.2490	0.9315
MobileNet	6	65	2.8701e-06	1.0	0.6174	0.9612

Validation Process

The follow-up to determine model performance is through a testing process, in this work, as a validation process for predictions from the two models. CNN has the fluctuations and the separation distance, between loss and validation loss are still high. In contrast to training-validation accuracy, the fluctuation is not too high even though the separation distance of the both are still quite high (Figure 7a). Figure 7b shows that MobileNet has the advantage in terms of very smooth fluctuations both in loss and accuracy, even though at the beginning of the epoch the fluctuations are still high, however, only at the initial spike, then it returns smoothly and achieves convergence (the point of stability). The difference between accuracy score training and validation is quite significant because it is still high.

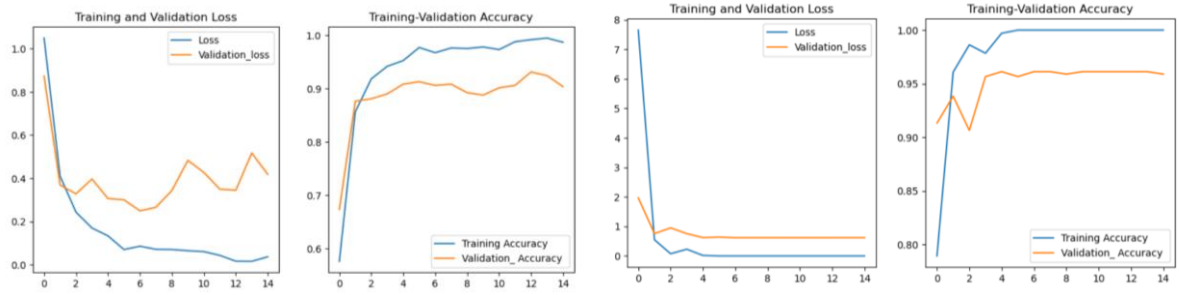

a. CNN b. MobileNet

Figure 7. Models Performance

Evaluation Process

The model requires evaluation as a measuring tool to determine its performance. Based on the Classification report as in Table 3, CNN precision has the highest value for COVID-19. However, the value is lower in the normal and virus classes. The accuracy value between COVID (0.99) and normal (0.93) and virus (0.91) has a fair difference. The recall and F1-score values are 0.93, 0.94, and 0.95 respectively; 0.96, 0.94, and 0.95 have small difference values. The average performance value is 0.94. The prediction results for COVID-19 images show that the images are recognized validly for 100 COVID-19 images, 121 normal, 12 viruses, and the other are errors in the distribution of false positive and false negative data.

The difference between CNN and MobileNet (Table 3 and Table 4) is fairly significant as shown in Table 3. MobileNet performance value of 0.97 outperforms CNN value of 0.94. The difference between the two is around 0.03 or 3%, which is quite significant. The MobileNet model also has fairly stable precision, recall, f1-score because the lowest is only 0.95 and the highest is 0.99. The prediction results succeeded in validly classifying 107 Covid images, 7 images were superior to CNN and for normal they were superior to CNN by 3 images. This proves that MobileNet has the best performance between the two as the value during training also outperforms CNN. This advantage indicates that the number of MobileNet parameters is greater than CNN, making it possible to carry out batch normalization which reduces the hyperparameter weights and provides unique values for each class. This gives MobileNet the ability to recognize images more validly than CNN. In addition, because of batch normalization, even though MobileNet has

more than the number of CNN parameters, it is able to produce a shorter step speed for running each epoch during the train process.

Table 3. Classification Reports

	CNN				MobileNet			
	Precision	***Recall***	***F1-Score***	***Support***	***Precision***	***Recall***	***F1-Score***	***Support***
0	0.99	0.93	0.96	108	0.98	0.99	0.99	108
1	0.93	0.94	0.93	129	0.96	0.96	0.96	129
2	0.91	0.95	0.93	128	0.96	0.95	0.96	128
Accuracy			0.94	365			0.97	365
Macro Avg	0.94	0.94	0.94	365	0.97	0.97	0.97	365
Wighted Avg	0.94	0.94	0.94	365	0.97	0.97	0.97	365

Table 4. Model Prediction

	CNN			MobileNet		
	COVID-19	***Normal***	***Virus***	***COVID-19***	***Normal***	***Virus***
Covid	100	3	5	107	0	1
Normal	1	121	7	1	124	4
Virus	0	6	122	1	5	122

Based on these results, the investigation of model performance on CXR image objects outperformed previous authors, including [32], [33], [34], [36].

Conclusion

This research succeeded in investigating and proving that MobileNet outperforms CNN even though MobileNet is also based on CNN. This advantage focuses on the layer arrangement and batch normalization which speeds up the step speed in the training process. This research still needs to be continued to investigate ensemble learning between CNN and MobileNet which has the opportunity to outperform these results. Ensembles for different models either combine two or more models so that limitations in each model can be overcome with short computing times or step speeds and low fluctuation values with stable convergence values.

Acknowledgement

Special thanks to Ministry of Education and Culture, Research, Technology, and Higher Education, Indonesia for support in funding of this research. Hopefully, it will be a connected access to increase the next level of research.

References

[1] A. P. Agustin, A. C. Fauzan, and Harliana, "Implementasi K-Nearest Neighbor Dengan Jarak Minkowski Untuk Deteksi Dini COVID-19 Pada Citra Ct-Scan Paru - Paru," *J. Ilm. Intech Inf. Technol. J. UMUS*, vol. 4, no. 1, pp. 23–30, 2022.

[2] Q. Li *et al.*, "Early Transmission Dynamics in Wuhan, China, of Novel Coronavirus–Infected Pneumonia," *N. Engl. J. Med.*, vol. 382, no. 13, pp. 1199–1207, 2020, doi: 10.1056/nejmoa2001316.

[3] Y. M. Arabi, S. Murthy, and S. Webb, "COVID-19: a novel coronavirus and a novel challenge for critical care," *Intensive Care Med.*, vol. 46, no. 5, pp. 833–836, 2020, doi: 10.1007/s00134-020-05955-1.

[4] M. Anthimopoulos, S. Christodoulidis, L. Ebner, A. Christe, and S. Mougiakakou, "Lung Pattern Classification for Interstitial Lung Diseases Using a Deep Convolutional Neural Network," *IEEE Trans. Med. Imaging*, vol. 35, no. 5, pp. 1207–1216, 2016, doi: 10.1109/TMI.2016.2535865.

[5] Y. Wang *et al.*, "Precise pulmonary scanning and reducing medical radiation exposure by developing a clinically applicable intelligent CT system: Toward improving patient care," *EBioMedicine*, vol. 54, 2020, doi: 10.1016/j.ebiom.2020.102724.

[6] K. Buys, C. Cagniart, A. Baksheev, T. De Laet, J. De Schutter, and C. Pantofaru, "An adaptable system for RGB-D based human body detection and pose estimation," *J. Vis. Commun. Image Represent.*, vol. 25, no. 1, pp. 39–52, 2014, doi: 10.1016/j.jvcir.2013.03.011.

[7] D. Selvaraj, A. Venkatesan, V. G. V. Mahesh, and A. N. Joseph Raj, "An integrated feature frame work for automated segmentation of COVID-19 infection from lung CT images," *Int. J. Imaging Syst. Technol.*, vol.

31, no. 1, pp. 28–46, 2021, doi: 10.1002/ima.22525.

[8] G. Jia, H. Lam, and Y. Xu, "Since January 2020 Elsevier has created a COVID-19 resource centre with free information in English and Mandarin on the novel coronavirus COVID- 19 . The COVID-19 resource centre is hosted on Elsevier Connect , the company ' s public news and information ," no. January, 2020.

[9] B. Abraham and M. S. Nair, "Computer-aided detection of COVID-19 from X-ray images using multi-CNN and Bayesnet classifier," *Biocybern. Biomed. Eng.*, vol. 40, no. 4, pp. 1436–1445, 2020, doi: 10.1016/j.bbe.2020.08.005.

[10] R. Karthik, R. Menaka, and M. Hariharan, "Learning distinctive filters for COVID-19 detection from chest X-ray using shuffled residual CNN," *Appl. Soft Comput.*, vol. 99, p. 106744, 2021, doi: 10.1016/j.asoc.2020.106744.

[11] A. Rehman, T. Sadad, T. Saba, A. Hussain, and U. Tariq, "Real-Time Diagnosis System of COVID-19 Using X-Ray Images and Deep Learning," *IT Prof.*, vol. 23, no. 4, pp. 57–62, 2021, doi: 10.1109/MITP.2020.3042379.

[12] R. Shrestha and L. Shrestha, "Coronavirus disease 2019 (COVID-19): A pediatric perspective," *J. Nepal Med. Assoc.*, vol. 58, no. 227, pp. 525–532, 2020, doi: 10.31729/jnma.4977.

[13] A. Abbas, M. M. Abdelsamea, and M. M. Gaber, "Classification of COVID-19 in chest X-ray images using DeTraC deep convolutional neural network," *Appl. Intell.*, vol. 51, no. 2, pp. 854–864, 2021, doi: 10.1007/s10489-020-01829-7.

[14] H. Shi *et al.*, "Radiological findings from 81 patients with COVID-19 pneumonia in Wuhan, China: a descriptive study," *Lancet Infect. Dis.*, vol. 20, no. 4, pp. 425–434, 2020, doi: 10.1016/S1473-3099(20)30086-4.

[15] B. Yanti and U. Hayatun, "Peran pemeriksaan radiologis pada diagnosis Coronavirus disease 2019," *J. Kedokt. Syiah Kuala*, vol. 20, no. 1, pp. 53–57, 2020, doi: 10.24815/jks.v20i1.18300.

[16] S. Hassantabar, M. Ahmadi, and A. Sharifi, "Diagnosis and detection of infected tissue of COVID-19 patients based on lung x-ray image using convolutional neural network approaches," *Chaos, Solitons & Fractals*, vol. 140, p. 110170, Nov. 2020, doi: 10.1016/J.CHAOS.2020.110170.

[17] S. Pathan, P. C. Siddalingaswamy, and T. Ali, "Automated Detection of COVID-19 from Chest X-ray scans using an optimized CNN architecture," *Appl. Soft Comput.*, vol. 104, p. 107238, 2021, doi: 10.1016/j.asoc.2021.107238.

[18] I. Sulistyowati and L. R. W. Utami, "Tingkat Kecemasan Radiografer dalam Memberikan Pelayanan Radiologi pada Masa Pandemi COVID-19 di Rumah Sakit Baitul Hikmah Kendal," *J. Ilmu dan Teknol. Kesehat. STIKES Widya Husada*, vol. 12, no. 2, pp. 55–61, 2021.

[19] S. Ahmad, "A Review of COVID-19 (Coronavirus Disease-2019) Diagnosis, Treatments and Prevention," *Eurasian J. Med. Oncol.*, vol. 2019, 2020, doi: 10.14744/ejmo.2020.90853.

[20] G. Wang, "A perspective on deep imaging," *IEEE Access*, vol. 4, pp. 8914–8924, 2016, doi: 10.1109/ACCESS.2016.2624938.

[21] E. Dandil, M. Cakiroglu, Z. Eksi, M. Ozkan, O. K. Kurt, and A. Canan, "Artificial neural network-based classification system for lung nodules on computed tomography scans," *6th Int. Conf. Soft Comput. Pattern Recognition, SoCPaR 2014*, pp. 382–386, 2014, doi: 10.1109/SOCPAR.2014.7008037.

[22] J. Kuruvilla and K. Gunavathi, "Lung cancer classification using neural networks for CT images," *Comput. Methods Programs Biomed.*, vol. 113, no. 1, pp. 202–209, 2014, doi: 10.1016/j.cmpb.2013.10.011.

[23] T. Manikandan and N. Bharathi, "Lung Cancer Detection Using Fuzzy Auto-Seed Cluster Means Morphological Segmentation and SVM Classifier," *J. Med. Syst.*, vol. 40, no. 7, 2016, doi: 10.1007/s10916-016-0539-9.

[24] P. B. Sangamithraa and S. Govindaraju, "Lung tumour detection and classification using EK-Mean clustering," *Proc. 2016 IEEE Int. Conf. Wirel. Commun. Signal Process. Networking, WiSPNET 2016*, pp. 2201–2206, 2016, doi: 10.1109/WiSPNET.2016.7566533.

[25] M. M. A. Asmaa Abbas, "Learning Trnasformations for Automated Classification of Manifestation of Tuberculosis using Convolutional Neural Network," in *2018 13th International Conference on Computer Engineering and Systems (ICCES)*, 2018, pp. 122–126, doi: 10.1109/ICCES.2018.8639200.

[26] W. Sun, B. Zheng, and W. Qian, "Computer aided lung cancer diagnosis with deep learning algorithms," *Med.*

Imaging 2016 Comput. Diagnosis, vol. 9785, p. 97850Z, 2016, doi: 10.1117/12.2216307.

[27] Y. Lecun, Y. Bengio, and G. Hinton, "Deep learning," *Nature*, vol. 521, no. 7553, pp. 436–444, 2015, doi: 10.1038/nature14539.

[28] J. Wan *et al.*, "Institutional Knowledge at Singapore Management University Deep learning for content-based image retrieval : A comprehensive study Chinese Academy of Sciences," 2014.

[29] L. Deng, "Deep Learning: Methods and Applications," *Found. Trends Signal Process.*, vol. 7, no. June 2014, pp. 197–387, 2014, doi: 10.1561/2000000039.

[30] H. Greenspan, B. Van Ginneken, and R. M. Summers, "Guest Editorial Deep Learning in Medical Imaging: Overview and Future Promise of an Exciting New Technique," *IEEE Trans. Med. Imaging*, vol. 35, no. 5, pp. 1153–1159, 2016, doi: 10.1109/TMI.2016.2553401.

[31] I. D. Maysanjaya, "Klasifikasi Pneumonia pada Citra X-rays Paru-paru dengan Convolutional Neural Network (Classification of Pneumonia Based on Lung X-rays Images using Convolutional Neural Network)," vol. 9, no. 2, pp. 190–195, 2020.

[32] L. A. Andika, H. Pratiwi, and S. S. Handajani, "Lingga Aji Andika 1 , Hasih Pratiwi 2 , and Sri Sulistijowati Handajani 3 1," pp. 331–340, 2019.

[33] A. B. Handoko, I. K. Timotius, D. Utomo, F. Teknik, U. Kristen, and S. Wacana, "Klasifikasi Citra X-Ray COVID-19 Menggunakan Three-layered CNN Model," no. April 2022, pp. 155–168.

[34] N. A. Baghdadi, A. Malki, S. F. Abdelaliem, H. Magdy, M. Badawy, and M. Elhosseini, "An automated diagnosis and classification of COVID-19 from chest CT images using a transfer learning-based convolutional neural network," vol. 144, no. January, 2022.

[35] A. G. Howard and W. Wang, "Applications," 2012.

[36] W. Wang, Y. Li, T. Zou, X. Wang, J. You, and Y. Luo, "A Novel Image Classification Approach via Dense-MobileNet Models," vol. 2020, 2020.

[37] S. Indolia, A. Kumar, S. P. Mishra, and P. Asopa, "ScienceDirect Conceptual Understanding of Convolutional Neural Network- A Deep Learning Approach," *Procedia Comput. Sci.*, vol. 132, pp. 679–688, 2018, doi: 10.1016/j.procs.2018.05.069.

[38] D. Valero-Carreras, J. Alcaraz, and M. Landete, "Comparing two SVM models through different metrics based on the confusion matrix," *Comput. Oper. Res.*, vol. 152, no. December 2022, p. 106131, 2023, doi: 10.1016/j.cor.2022.106131.

[39] K. Parang, L. Wiebe, and E. Knaus, *Novel Approaches for Designing 5-O-Ester Prodrugs of 3-Azido-2,3-dideoxythymidine (AZT).*, vol. 7, no. 10. 2012.